Optica Applicata, Vol. XLVIII, No. 3, 2018
10.5277/oa180302

Defect solitons supported by kagome photonic lattices in biased photovoltaic-photorefractive crystals

JUANLI HUI[1, 2], KEQING LU[1, 2*], CHONG ZHAO[1, 2], LIXU GAO[1, 2], WEIJUN CHEN[1, 2]

[1]Tianjin Key Laboratory of Optoelectronic Detection Technology and Systems, Tianjin Polytechnic University, Tianjin 300387, China

[2]School of Electronics and Information Engineering, Tianjin Polytechnic University, Tianjin 300387, China

*Corresponding author: kqlutj@126.com

We report that defect solitons can be supported by kagome photonic lattices with a defect in biased photovoltaic-photorefractive crystals. For a positive defect, these defect solitons exist only in the semi-infinite bandgap and are stable in the low power region but unstable in the high power region. For a negative defect, these defect solitons exist in both of the semi-infinite bandgaps and the first bandgap. In the semi-infinite bandgap, low-power defect solitons are stable when the negative defect depth is low and unstable when the negative defect depth is high, moderate-power defect solitons are stable when the negative defect depth is high, and high-power defect solitons are unstable for all the negative defect depths. In the first bandgap, defect solitons are stable in all the power regions when the negative defect depth is low. When the negative defect depth is high, defect solitons are stable in the high power region and unstable in the low power region. On the other hand, these defect solitons are those studied previously in kagome photonic lattices with a defect in biased non-photovoltaic-photorefractive crystals when the bulk photovoltaic effect is negligible and those in kagome photonic lattices with a defect in photovoltaic-photorefractive crystals when the external bias field is absent.

Keywords: defect solitons, photonic lattices, photorefractive nonlinearity, nonlinear optics.

1. Introduction

Study of light propagation in periodic optical systems such as waveguide arrays, photonic lattices, and photonic crystals has attracted growing interest due to its physics and light -routing applications. The unique feature of such periodic systems is the existence of Bloch bands and forbidden bandgaps in the linear spectrum. On the other hand, when the forward- and backward-propagating waves experience Bragg scattering from periodic structures, their nonlinear coupling can produce gap solitons, which can exist in different bandgaps. Photonic lattices can support different kinds of gap solitons under different nonlinearities. At present, a wide variety of solitons in uniformly periodic

photonic lattices are known: fundamental solitons [1–7], vortex solitons [8–12], dipole solitons [13, 14], reduced-symmetry solitons [15], embedded-soliton trains [16], and so on, many of which have been experimentally observed. Of particular interest is a defect in the periodic medium which supports surface defect solitons [17, 18], defect modes (DMs), and defect solitons (DSs) in bandgaps of the periodic medium. DMs in photonic lattices in biased non-photovoltaic-photorefractive (non-PP) [19–21], PP [22], and biased PP [23] crystals have been proposed. On the other hand, DSs in one-dimensional photonic lattices [24], two-dimensional square photonic lattices [25], and kagome photonic lattices [26] have been predicted in biased non-PP crystals. However, DSs in optically induced kagome photonic lattices in biased PP crystals have not been investigated yet.

In this paper, we report on that DSs in optically induced kagome photonic lattices with a defect in biased PP crystals can exist in different bandgaps when the defect strength is changed. The existential region of these DSs decreases with an increase in the positive defect strength and increases with the negative defect depth. For a positive defect, DSs exist only in the semi-infinite bandgap and are stable in the low power region but unstable in the high power region. For a negative defect, DSs exist in the semi-infinite and first bandgaps. In the semi-infinite bandgap, low-power DSs are stable when the negative defect depth is low but unstable when the negative defect depth is high, moderate-power DSs are stable when the negative defect depth is high, and high-power DSs are unstable for the all the negative defect depths. In the first bandgap, when the negative defect depth is low, DSs are stable in the all power region, whereas when the negative defect depth is high, high-power DSs are stable and low-power DSs are unstable. When the bulk photovoltaic effect is negligible, these DSs are those studied previously in kagome photonic lattices with a defect in biased non-PP crystals. When the external bias field is absent, these DSs are those in kagome photonic lattices with a defect in PP crystals.

2. Theoretical model

Let us consider the physical situation in which an ordinarily polarized beam through a mask is launched into a biased PP crystal. The mask can control the distribution of optical intensity that forms a kagome lattice beam with a defect. This defected lattice beam is assumed to be uniform along the direction of propagation. Meanwhile, an extraordinarily polarized probe beam is launched into the defect site, propagating collinearly with the lattice beam. The probe beam at the defect site in kagome optical lattices in the biased PP crystal is described by the nonlinear Schrödinger equation [23, 26]:

$$i\frac{\partial U}{\partial z}+\frac{\partial^2 U}{\partial x^2}+\frac{\partial^2 U}{\partial y^2}-E_0\frac{1}{I_L+|U|^2+1}U+E_p\frac{I_L+|U|^2}{I_L+|U|^2+1}U=0 \qquad (1)$$

where U is the slowly varying amplitude of the probe beam, z is the propagation distance (in units of $2kT^2/\pi^2$), T is the lattice spacing, $k=2\pi n_e/\lambda$ is the optical wave num-

ber in the PP crystal, n_e is the unperturbed extraordinary index of refraction, λ is the wavelength, x and y are the transverse distances (in units of T/π), E_0 is the applied dc field (in units of $\pi^2/(T^2k^2n_e^4r_{33})$) [21], r_{33} is the electro-optic coefficient, E_p is the photovoltaic field constant (in units of $\pi^2/(T^2k^2n_e^4r_{33})$) [23], I_L is the intensity function of the photonic lattices described by [21, 26]

$$I_L = I\left\{1 + \varepsilon \exp\left[\frac{-(4x^2 + 3y^3)^4}{128}\right]\right\} \tag{2}$$

where I is the intensity profile of kagome lattices as described by [27]

$$I = V_0\left|2\exp\left(\frac{ik_1py}{1+4p/3}\right)\cos\left(\frac{k_1py}{1+4p/3}\right)\exp\left(\frac{ik_1y}{1+4p/3}\right) + \exp\left(\frac{-ik_1y}{2(1+4p/3)} - \frac{i\sqrt{3}}{2}k_1x\right) + \exp\left(\frac{-ik_1y}{2(1+4p/3)} + \frac{i\sqrt{3}}{2}k_1x\right)\right|^2 \tag{3}$$

and $p = 3/2$ (note that when $p = 3/2$, the lattice transforms from the well-known honeycomb interference pattern into the richer kagome lattice), V_0 is the lattice peak intensity, $k_1 = 4\pi/d$ is the periodicity in the x direction, and ε controls the strength of the defect. For a positive defect ($\varepsilon > 0$), the lattice light intensity I_L at the defect site is higher than that at the surrounding sites. For a negative defect ($\varepsilon < 0$), the lattice intensity I_L at the defect site is lower than that at the surrounding sites. Figure 1**a** depicts the intensity distribution of kagome lattices. In this paper, we consider the following examples: let $T = 20$ μm, $V_0 = 0.375$, $d = \sqrt{3}\pi$, and $\lambda = 0.5$ μm [26, 27]. Let the PP crystal be $BaTiO_3$ [28] with the parameters $n_e = 2.365$, $r_{33} = 80 \times 10^{-12}$ m/V, and the actual photovoltaic field constant $E_p' = 5$ kV/cm [29]. For this set of values, we find that $E_p \approx 8$ and that one E_0 or E_p unit corresponds to 62 V/mm, one x or y unit corresponds to 6.4 μm, and one z unit corresponds to 2.4 mm in physical units. For illustration purposes, we take $E_0 = 25$.

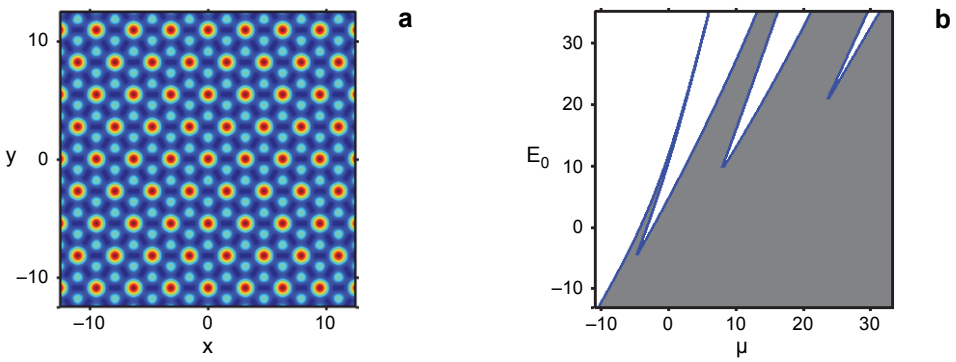

Fig. 1. The kagome photonic lattices (**a**). Band structure of kagome photonic lattices (**b**).

In order to show the existent conditions for DSs, let us first understand the dispersion relation and bandgap structure of the linear version of Eq. (1). According to the Bloch theorem, eigenfunctions of the linear version of Eq. (1) can be sought in the form $U(x, y, z) = u(x, y)\exp[i(k_x x + k_y y - \mu z)]$, where $u(x, y)$ is a periodic function with the same periodicity as the lattices, k_x and k_y are wave numbers in the first Brillouin zone, and μ is the Bloch-wave propagation constant. Direct substitution of this form of $U(x, y, z)$ in the linear version of Eq. (1) yields the following eigenvalue equation

$$\frac{\partial^2 u}{\partial x^2} + \frac{\partial^2 u}{\partial y^2} + 2ik_x\frac{\partial u}{\partial x} + 2ik_y\frac{\partial u}{\partial y} - (k_x^2 + k_y^2)u + V(x, y)u = -\mu u \tag{4}$$

where $V(x, y) = (E_p I - E_0)/(1 + I)$ is the uniform periodic potential. We calculate Eq. (4) by the plane wave expansion method to obtain the bandgap diagram as shown in Fig. 1**b**. When $E_0 = 25$ in Fig. 1**b**, we obtain the regions of the semi-infinite, first, second, and third gaps as $\mu < 3.49$, $3.56 < \mu < 8.99$, $12.83 < \mu < 16.14$, and $25.35 < \mu < 25.74$, respectively.

We obtain the solution of Eq. (1) for stationary solitons in the form of $U(x, y, z) = u(x, y)\exp(-i\mu z)$, where $u(x, y)$ is a localized function in x and y. Substituting this form of $U(x, y, z)$ into Eq. (1), we find that

$$\frac{\partial^2 u}{\partial x^2} + \frac{\partial^2 u}{\partial y^2} - E_0\frac{1}{I_L + u^2 + 1}u + E_p\frac{I_L + u^2}{I_L + u^2 + 1}u = -\mu u \tag{5}$$

from which DSs $u(x, y)$ can be obtained by a numerical method. Such a numerical method is to expand the solution $u(x, y)$ into discrete Fourier series and then convert Eq. (5) into a matrix eigenvalue problem with μ as the eigenvalue [30]. The power of DSs is defined as

$$P = \int_{-\infty}^{\infty}\int_{-\infty}^{\infty} u^2\,\mathrm{d}x\,\mathrm{d}y$$

To analyze the stability of DSs, they are perturbed as

$$U(x, y, z) = \Big\{u(x, y) + \Big[v(x, y) - w(x, y)\Big]\exp(\delta z) + \Big[v(x, y) + w(x, y)\Big]^*\exp(\delta^* z)\Big\}\exp(-i\mu z) \tag{6}$$

where the superscript * represents complex conjugation, and $v(x, y)$, $w(x, y) \ll 1$ are the small perturbations. By substituting Eq. (6) into Eq. (1) and linearizing the resulting equation, the eigenvalue equations are obtained as follows:

$$\delta v = -i\left(\mu w + \frac{\partial^2 w}{\partial x^2} + \frac{\partial^2 w}{\partial y^2} - E_0\frac{1}{I_L + u^2 + 1}w + E_p\frac{I_L + u^2}{I_L + u^2 + 1}w\right) \tag{7}$$

$$\delta w = -i\left[\mu v + \frac{\partial^2 v}{\partial x^2} + \frac{\partial^2 v}{\partial y^2} - E_0 \frac{I_L - u^2 + 1}{(I_L + u^2 + 1)^2} v \right.$$
$$\left. + E_p \frac{(I_L + u^2 + 1)^2 - I_L + u^2 - 1}{(I_L + u^2 + 1)^2} v \right] \tag{8}$$

which we solved by a numerical method that is called OOM [31]. If there exists $\mathrm{Re}(\delta) > 0$, DS is linearly unstable. Otherwise it is linearly stable. To test the predictions of linear stability analysis, we solved Eq. (1) numerically with the input conditions $U(x, y, z = 0) = w(x, y)[1 + \varphi(x, y)]$, where $\varphi(x, y)$ is a Gaussian random function with $\langle\varphi\rangle = 0$ and $\langle\varphi^2\rangle = \sigma^2$ (we choose that σ^2 is equal to the white noise with $\sigma^2 = 0.01$).

3. Numerical results

Let us first consider DSs for a positive defect ($\varepsilon > 0$). We find that DSs exist only in the semi-infinite bandgap. Figure 2**a** shows the power diagrams of DSs for three different values of the defect strength parameter ε, where dotted curve represents unstable DSs and solid, dashed, and dash-dot curves represent stable DSs. This figure demonstrates that the power of DSs decreases with an increase in the positive defect strength for a given propagation constant and the propagation constant for a given positive defect strength and that the existential region of DSs decreases with an increase in the positive defect strength. Figure 2**b** shows the real parts of perturbation growth rates $\mathrm{Re}(\delta)$ *vs.* the propagation constant for $\varepsilon = 0.2$, 0.5, and 0.8. It reveals that the stable region of DSs

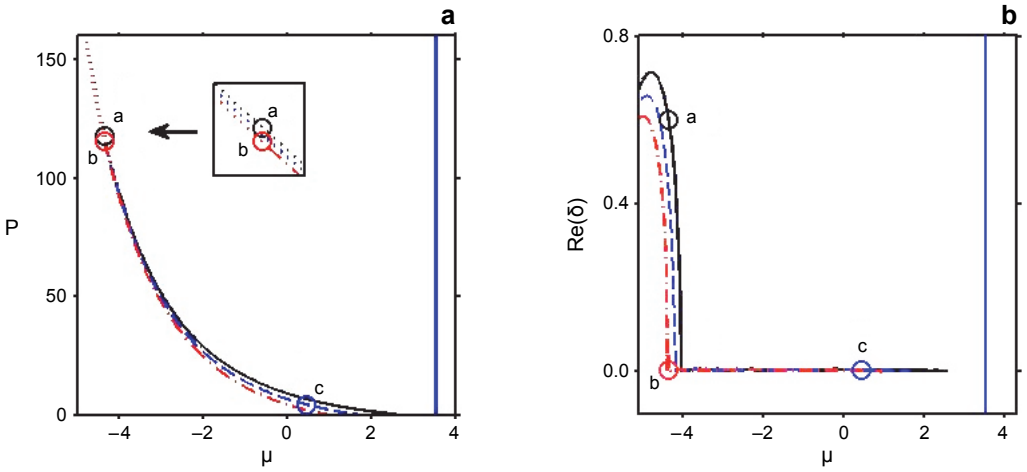

Fig. 2. Power *vs.* propagation constant μ (blue region is Bloch band) when $\varepsilon = 0.2$ (solid curve), $\varepsilon = 0.5$ (dashed curve), and $\varepsilon = 0.8$ (dash-dot curve); the solid, dashed, and dash-dot curves indicate the stable DSs, and the dot curve indicates the unstable DSs (**a**). Perturbation growth rates $\mathrm{Re}(\delta)$ corresponding to **a** (**b**). Profiles of DSs at the points *a*, *b*, and *c* are shown in Fig. 3.

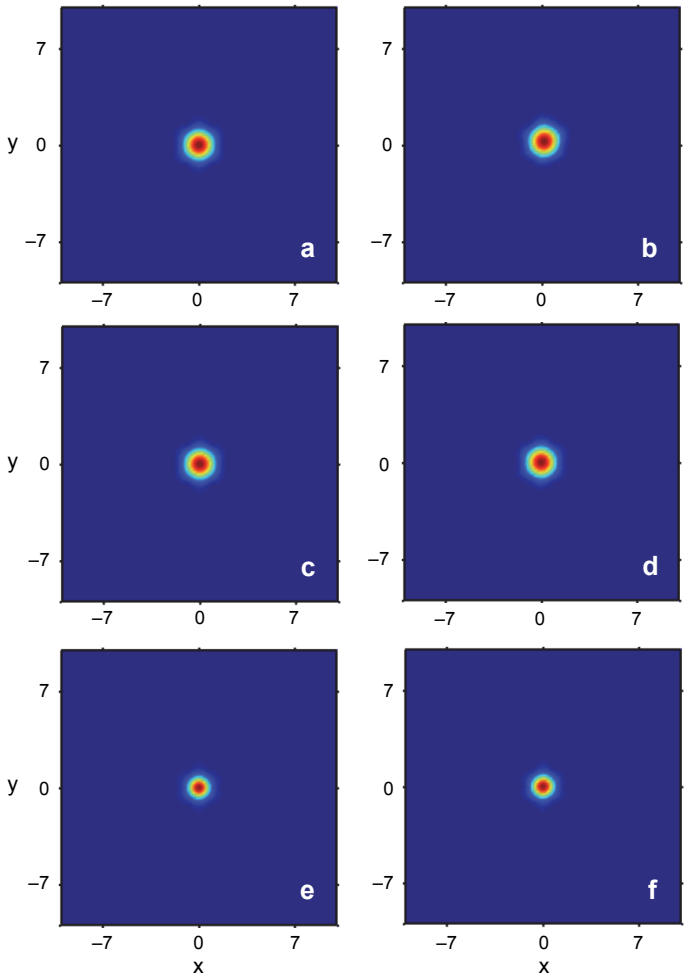

Fig. 3. Profile of DS at point *a* in Figs. 2**a** and 2**b** with $(\varepsilon, \mu) = (0.2, -4.37)$ (**a**), and its profile at $z = 300$ (**b**). Profile of DS at point *b* in Figs. 2**a** and 2**b** with $(\varepsilon, \mu) = (0.8, -4.37)$ (**c**) and its profile at $z = 300$ (**d**). Profile of DS at point *c* in Figs. 2**a** and 2**b** with $(\varepsilon, \mu) = (0.5, 0{,}43)$ (**e**) and its profile at $z = 300$ (**f**). The DS in (**a**) is unstable, while the DSs in (**c**) and (**e**) are stable.

decreases with an increase in positive defect strength. When $\mu < -4.05$ with $\varepsilon = 0.2$, $\mu < -4.20$ with $\varepsilon = 0.5$, and $\mu < -4.41$ with $\varepsilon = 0.8$ (corresponding to high power) in Fig. 2**a**, DSs cannot stably exist according to the diagram of growth rates $\mathrm{Re}(\delta)$ as shown in Fig. 2**b**. As an example, Fig. 3**a** shows the profile of a DS for $\mu = -4.37$ with $\varepsilon = 0.2$ (point *a* in Figs. 2**a** and 2**b**). Figure 3**b** shows the profile of the DS at $z = 300$, where the DS changes its original shape and place. When $-4.05 \le \mu \le 2.56$ with $\varepsilon = 0.2$, $-4.20 \le \mu \le 1.60$ with $\varepsilon = 0.5$, and $-4.41 \le \mu \le 0.94$ with $\varepsilon = 0.8$ (corresponding to low power) in Fig. 2**a**, DSs can stably exist (see Fig. 2**b**). For $\mu = -4.37$ with $\varepsilon = 0.8$ (point *b* in Figs. 2**a** and 2**b**) and $\mu = 0.43$ with $\varepsilon = 0.5$ (point *c* in Figs. 2**a** and 2**b**), the profiles of DSs are shown in Figs. 3**c** and 3**e**, whereas their profiles at $z = 300$ are dis-

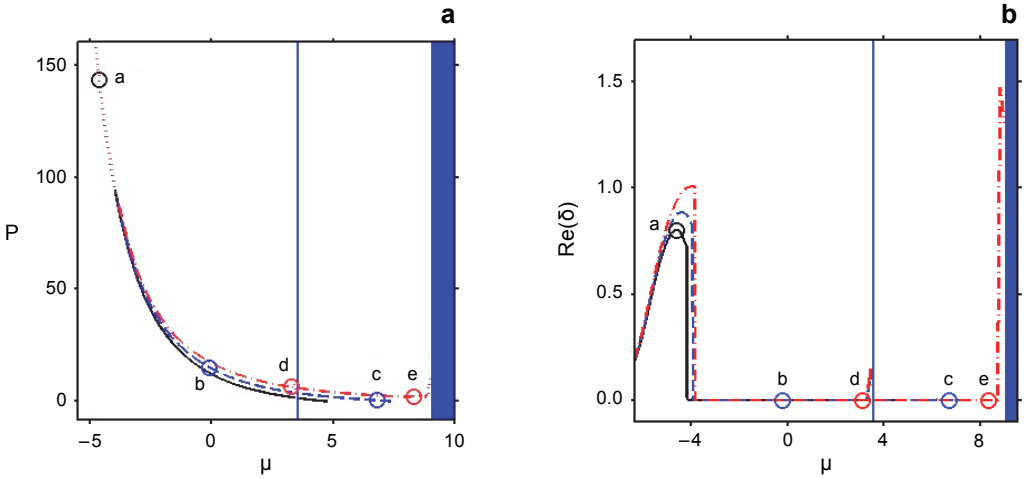

Fig. 4. Power *vs*. propagation constant (blue regions are Bloch band) when $\varepsilon = -0.2$ (solid curve), $\varepsilon = -0.5$ (dashed curve), and $\varepsilon = -0.8$ (dash-dot curve); the solid, dashed, and dash-dot curves indicate the stable DSs, and the dot curves indicate the unstable DSs (**a**). Perturbation growth rates Re(δ) corresponding to **a** (**b**). Profiles of DSs at the points *a*, *b*, *c*, *d* and *e* are shown in Fig. 5.

played in Figs. 3**d** and 3**f**. Evidently, DSs are stable since they propagate unchanged. The above results are in agreement with the growth rates in Fig. 2**b**.

Next, we consider the case of negative defect depths. In this case, DSs exist in the semi-infinite and first bandgaps. Figure 4**a** depicts the power diagrams of DSs for $\varepsilon = -0.2$, -0.5, and -0.8. This figure also shows that the power of DSs increases with the negative defect depth for a given propagation constant and decreases with an increase in the propagation constant for a given negative defect depth and that the stable region of DSs increases with the negative defect depth. The perturbation growth rates Re(δ) corresponding to Fig. 4**a** are shown in Fig. 4**b**. In the semi-infinite bandgap, when $3.30 < \mu < 3.40$ with $\varepsilon = 0.5$ and $3.30 < \mu < 3.43$ with $\varepsilon = 0.8$ in Fig. 4**a**, where the power of DSs is low, DSs are unstable because of Re(δ) > 0 (see Fig. 4**b**). Moreover, when $\mu < -4.10$ with $\varepsilon = -0.2$, $\mu < -3.93$ with $\varepsilon = -0.5$, and $\mu < -3.84$ with $\varepsilon = -0.8$ in Fig. 4**a**, where the power of DSs is high, DSs are also unstable (see Fig. 4**b**). As an example, taking $\mu = -4.65$ with $\varepsilon = -0.2$ (point *a* in Figs. 4**a** and 4**b**), the profile of a DS is displayed in Fig. 5**a** and its profile at $z = 300$ is shown in Fig. 5**b**. The DS at $z = 300$ changes its original shape and place, which is in agreement with the growth rate in Fig. 4**b**. When $-4.10 \le \mu \le 3.40$ with $\varepsilon = -0.2$ in Fig. 4**a**, where the power of DSs is low, DSs are stable because of Re(δ) $\not> 0$ (see Fig. 4**b**). When $-3.93 \le \mu \le 3.30$ with $\varepsilon = -0.5$ and $-3.84 \le \mu \le 3.30$ with $\varepsilon = -0.8$ in Fig. 4**a**, where the power of DSs is moderate, DSs are stable (see Fig. 4**b**). For example, for $\mu = -0.12$ with $\varepsilon = -0.5$ (point *b* in Figs. 4**a** and 4**b**) and $\mu = 3.26$ with $\varepsilon = -0.8$ (point *d* in Figs. 4**a** and 4**b**), Figs. 5**c** and 5**d** show the profiles of DSs, respectively. In the first bandgap, DSs with $\varepsilon = -0.2$ and -0.5 can stably exist in the all the power regions (see Fig. 4**b**). For $\varepsilon = -0.8$, DSs are stable in the region of $3.60 \le \mu \le 8.70$ corresponding to high power (see Fig. 4**b**)

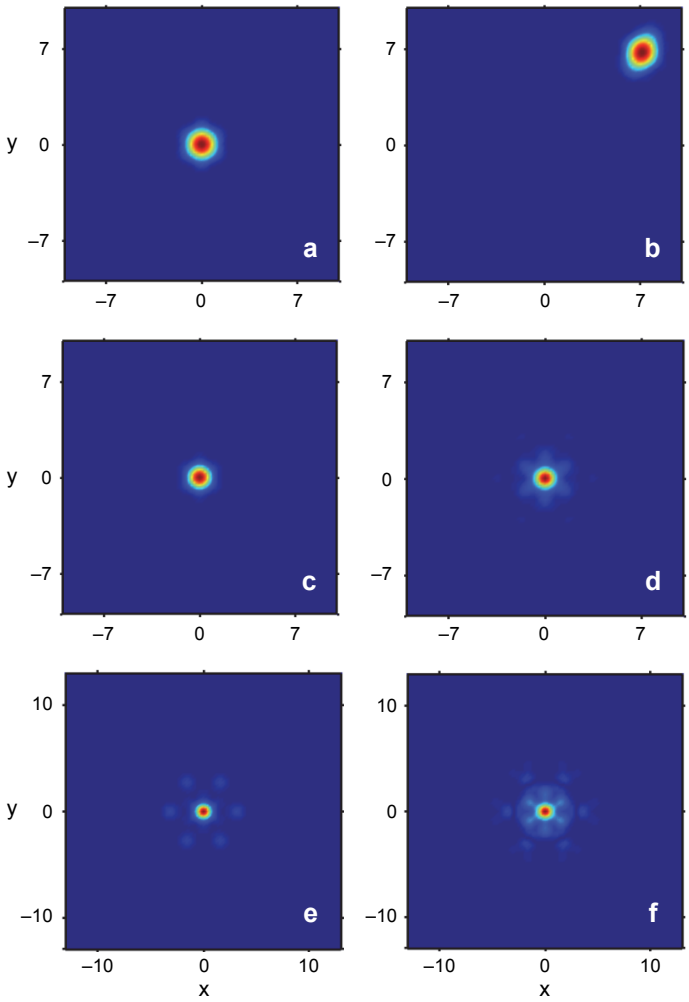

Fig. 5. Profile of DS at point *a* in Fig. 4**a** with (ε, μ) = (–0.2, –4.65) (**a**), and its profile at z = 300 (**b**). Profiles of DSs at points *b*, *c*, *d*, *e* in Fig. 4**a**, with (ε, μ) = (–0.5, –0.12), (ε, μ) = (–0.5, 6.78), (ε, μ) = = (–0.8, 3.26), and (ε, μ) = (–0.8, 8.29), respectively (**c**–**f**). The DS in (**a**) is unstable, while the DSs in (**c**–**f**) are stable.

but unstable in the region of $8.70 < \mu < 8.93$ corresponding to low power (see Fig. 4**b**). Taking μ = 6.78 with ε = –0.5 (point *c* in Figs. 4**a** and 4**b**) and μ = 8.29 with ε = –0.8 (point *e* in Figs. 4**a** and 4**b**), the profiles of the stable DSs are shown in Figs. 5**e** and 5**f**.

Finally, let us discuss the properties of DSs in optically induced kagome photonic lattices with a defect in biased PP crystals. When the bulk photovoltaic effect is negligible, *i.e.*, E_p = 0, our physical system becomes the physical system of DSs studied previously in optically induced kagome photonic lattices with a defect in biased non-PP crystals. In this case, Eqs. (1) and (5) lead to the same expressions (1) and (2) in [26], in which DSs have been investigated in optically induced kagome photonic lattices

with a defect in biased non-PP crystals. Moreover, substitution of $E_p = 0$ into Eqs. (7) and (8) yields the same coupled equations to get Re(δ) in [26]. The above results show that our theoretical model is correct. When the external bias field is absent, *i.e.*, $E_0 = 0$, our physical system becomes the physical system of DSs in optically induced kagome photonic lattices with a defect in PP crystals. In this case, from Eqs. (1)–(8) DSs can be obtained in optically induced kagome photonic lattices with a defect in PP crystals.

4. Conclusion

In conclusion, we have investigated DSs and their stability in optically induced kagome photonic lattices with a defect in biased PP crystals. We have shown that these DSs exist only in the semi-infinite bandgap for a positive defect and both in the semi-infinite bandgap and the first bandgap for a negative defect. Our analysis indicates that for a positive defect, low-power DSs are stable and high-power DSs are unstable, and that for a negative defect in the semi-infinite bandgap, low-power DSs are stable when the negative defect depth is low but unstable when the negative defect depth is high, moderate-power DSs are stable when the negative defect depth is high, and high-power DSs are unstable for the the negative defect depths; in the first bandgap, when the negative defect depth is low, DSs are stable in all the power regions and when the negative defect depth is high, high-power DSs are stable and low-power DSs are unstable. We have demonstrated that the stable region of these DSs decreases with an increase in the positive defect strength and increases with the negative defect depth. The properties of these DSs have been discussed and we have found that they are those studied previously in kagome photonic lattices with a defect in biased non-PP crystals when the bulk photovoltaic effect is negligible and those in kagome photonic lattices with a defect in PP crystals when the external bias field is absent.

Acknowledgements – The work was supported by the Natural Science Foundation of Chinese Tianjin (No. 13JCYBJC16400).

References

[1] Eisenberg H.S., Silberberg Y., Morandotti R., Boyd A.R., Aitchison J.S., *Discrete spatial optical solitons in waveguide arrays*, Physical Review Letters 81(16), 1998, p. 3383.

[2] Jianke Yang, Musslimani Z.H., *Fundamental and vortex solitons in a two-dimensional optical lattice*, Optics Letters 28(21), 2003, pp. 2094–2096.

[3] Efremidis N.K., Hudock J., Christodoulides D.N., Fleischer J.W., Cohen O., Segev M., *Two-dimensional optical lattice solitons*, Physical Review Letters 91(21), 2003, article ID 213906.

[4] Pelinovsky D.E., Sukhorukov A.A., Kivshar Yu.S., *Bifurcations and stability of gap solitons in periodic potentials*, Physical Review E 70(3), 2004, article ID 036618.

[5] Louis P.J.Y., Ostrovskaya E.A., Savage C.M., Kivshar Yu.S., *Bose–Einstein condensates in optical lattices: band-gap structure and solitons*, Physical Review A 67(1), 2003, article ID 013602.

[6] Efremidis N.K., Christodoulides D.N., *Lattice solitons in Bose–Einstein condensates*, Physical Review A 67(6), 2003, article ID 063608.

[7] IWANOW R., SCHIEK R., STEGEMAN G.I., PERTSCH T., LEDERER F., MIN Y., SOHLER W., *Observation of discrete quadratic solitons*, Physical Review Letters 93(11), 2004, article ID 113902.
[8] BAIZAKOV B.B., MALOMED B.A., SALERNO M., *Multidimensional solitons in periodic potentials*, EPL (Europhysics Letters) **63**(5), 2003, pp. 642–648.
[9] NESHEV D.N., ALEXANDER T.J., OSTROVSKAYA E.A., KIVSHAR YU.S., MARTIN H., MAKASYUK I., ZHIGANG CHEN, *Observation of discrete vortex solitons in optically induced photonic lattices*, Physical Review Letters 92(12), 2004, article ID 123903.
[10] FLEISCHER J.W., BARTAL G., COHEN O., MANELA O., SEGEV M., HUDOCK J., CHRISTODOULIDES D.N., *Observation of vortex-ring "discrete" solitons in 2D photonic lattices*, Physical Review Letters 92(12), 2004, article ID 123904.
[11] MALOMED B.A., KEVREKIDIS P.G., *Discrete vortex solitons*, Physical Review E 64(2), 2001, article ID 026601.
[12] ALEXANDER T.J., SUKHORUKOV A.A., KIVSHAR YU.S., *Asymmetric vortex solitons in nonlinear periodic lattices*, Physical Review Letters 93(6), 2004, article ID 063901.
[13] NESHEV D., OSTROVSKAYA E., KIVSHAR YU.S., KROLIKOWSKI W., *Spatial solitons in optically induced gratings*, Optics Letters 28(9), 2003, pp. 710–712.
[14] JIANKE YANG, MAKASYUK I., BEZRYADINA A., ZHIGANG CHEN, *Dipole and quadrupole solitons in optically induced two-dimensional photonic lattices: theory and experiment*, Studies in Applied Mathematics 113(4), 2004, pp. 389–412.
[15] FISCHER R., TRÄGER D., NESHEV D.N., SUKHORUKOV A.A., KROLIKOWSKI W., DENZ C., KIVSHAR YU.S., *Reduced-symmetry two-dimensional solitons in photonic lattices*, Physical Review Letters 96(2), 2006, article ID 023905.
[16] XIAOSHENG WANG, ZHIGANG CHEN, JIANDONG WANG, JIANKE YANG, *Observation of in-band lattice solitons*, Physical Review Letters 99(24), 2007, article ID 243901.
[17] KARTASHOV Y.V., VYSLOUKH V.A., TORNER L., *Surface lattice solitons in diffusive nonlinear media*, Optics Letters 33(8), 2008, pp. 773–775.
[18] JUANLI HUI, KEQING LU, BAOJU ZHANG, JUN ZHANG, HAIYING XING, *Surface defect lattice solitons in biased photovoltaic–photorefractive crystals*, Optics and Laser Technology 75, 2015, pp. 57–62.
[19] FEDELE F., JIANKE YANG, ZHIGANG CHEN, *Defect modes in one-dimensional photonic lattices*, Optics Letters 30(12), 2005, pp. 1506–1508.
[20] XIAOSHENG WANG, JACK YOUNG, ZHIGANG CHEN, WEINSTEIN D., JIANKE YANG, *Observation of lower to higher bandgap transition of one-dimensional defect modes*, Optics Express 14(16), 2006, pp. 7362–7367.
[21] JIANDONG WANG, JIANKE YANG, ZHIGANG CHEN, *Two-dimensional defect modes in optically induced photonic lattices*, Physical Review A 76(1), 2007, article ID 013828.
[22] KEHAO LI, KEQING LU, JIANBANG GUO, WEIJUN CHEN, TONGTONG SUN, FENGXUE YAO, JINGJUN XU, *Defect modes supported by optical lattices in photovoltaic-photorefractive crystals*, Optics Communications 285(13–14), 2012, pp. 3187–3190.
[23] KEQING LU, JIANBANG GUO, KEHAO LI, WEIJUN CHEN, TONGTONG SUN, FENGXUE YAO, PINGJUAN NIU, JINGJUN XU, *Defect modes in optically induced photonic lattices in biased photovoltaic–photorefractive crystals*, Optical Materials 34(8), 2012, pp. 1277–1281.
[24] JIANKE YANG, ZHIGANG CHEN, *Defect solitons in photonic lattices*, Physical Review E 73(2), 2006, article ID 026609.
[25] CHEN W.H., ZHU X., WU T.W., LI R.H., *Defect solitons in two-dimensional optical lattices*, Optics Express 18(11), 2010, pp. 10956–10962.
[26] XING ZHU, HONG WANG, LI-XIAN ZHENG, *Defect solitons in kagome optical lattices*, Optics Express 18(20), 2010, pp. 20786–20792.
[27] LAW K.J.H., SAXENA A., KEVREKIDIS P.G., BISHOP A.R., *Localized structures in kagome lattices*, Physical Review A 79(5), 2009, article ID 053818.
[28] STURMAN B.I., FRIDKIN V.M., *The Photovoltaic and Photorefractive Effect in Non-centrosymmetric Materias*, Gordon and Breach, Philadelphia, 1992.

[29] KEHAO LI, KEQING LU, YIQI ZHANG, PINGJUAN NIU, LIYUANYU, YANPENG ZHANG, *Localized surface waves at the interfzace between a linear dielectric and a photovoltaic-photorefractive crystal*, Optics and Laser Technology 48, 2013, pp. 79–82.

[30] JIANKE YANG, LAKOBA T.I., *Universally-convergent squared-operator iteration methods for solitary waves in general nonlinear wave equations*, Studies in Applied Mathematics 118(2), 2007, pp. 153–197.

[31] JIANKE YANG, *Iteration methods for stability spectra of solitary waves*, Journal of Computational Physics 227(14), 2008, pp. 6862–6876.

Received July 27, 2017